NJC

ROYAL SOCIETY OF CHEMISTRY

PAPER

View Article Online
View Journal | View Issue

Cite this: *New J. Chem.*, 2021, **45**, 21881

Novel anthracene-based organic dyes as co-sensitizers of porphyrins for developing efficient dye-sensitized solar cells†

Yunyu Tang,‡[a] Guangxin Yang,‡[a] Xiaoyi Lou,[a] Chengjie Li,[b] Dongmei Huang*[a] and Yongshu Xie*[b]

Received 7th October 2021,
Accepted 20th October 2021

DOI: 10.1039/d1nj04797c

rsc.li/njc

To develop cosensitizers for fabricating dye-sensitized solar cells (DSSCs) based on porphyrin dyes, **C2** and **C3** have been synthesized using a diphenylamine donor, an anthracene based π-spacer and a benzoic acid acceptor on the basis of our previously reported cosensitizer **C1**. Thus, two hexyloxy chains have been introduced in the diphenylamine donor to synthesize **C2** with the purpose of extending the absorption wavelength range and suppressing the charge recombination, and **C3** has been synthesized by introducing two bulky 2,4-bis(hexyloxy)phenyl groups in the diphenylamine donor to effectively suppress dye aggregation and charge recombination between the injected electrons and the electrolyte. On this basis, DSSCs have been fabricated by using **C1–C3** based on the cobalt electrolyte. As expected, an obviously higher J_{sc} of 13.03 mA cm^{-2} has been obtained for **C2** relative to that of 11.92 mA cm^{-2} obtained for **C1**. As a result, **C2** shows a slightly improved efficiency of 7.59%. On the other hand, the molecular structure of **C3** has been further optimized with two bulky dihexyloxyphenyl units, and thus the suppressed interfacial back electron transfer improves the J_{sc} to 13.23 mA cm^{-2} and the superior anti-aggregation ability enhances the V_{oc} to 857 mV. Finally, the highest PCE value of 8.95% is achieved for **C3**. On this basis, cosensitization with **XW66** affords remarkable efficiencies of 9.06%, 9.89% and 10.22% for **C1–C3**, respectively. These results provide an effective approach for developing efficient cosensitizers for porphyrins by introducing suitable substituents into the donor unit.

Introduction

The increasing global energy demand and environmental pollution problems have inspired scientists to explore renewable sources of energy. Among them, solar energy is the most abundant source of alternative, clean and pollution-free energy. Since the initial work in 1991, dye-sensitized solar cells (DSSCs) have been extensively explored owing to their relatively low cost, easy fabrication, good flexibility and high efficiency.[1–4]

To date, excellent dyes mainly include ruthenium complex sensitizers,[5,6] metal-free organic dyes[7–9] and porphyrin dyes.[10–17] Among them, porphyrin-based donor–π–acceptor (D–π–A) dyes have been demonstrated to be efficient due to their excellent light-harvesting ability and easy structure modulation, and thus a number of porphyrin dyes with high performance have been developed.[18–21] Despite the successful examples, porphyrin sensitizers have obvious weak absorption within the wavelength ranges of 500–600 nm and 350–410 nm, which hampers the further improvement of the efficiencies.[22–25] On the other hand, good planarity of a large conjugated framework leads to severe dye aggregation and π···π stacking on the TiO_2 surface, which will quench the excited dyes and thus diminish electron injection.[26–28] To address these problems, cosensitizers with complementary absorption characters have been designed for improving light harvesting by filling up the absorption valleys of the porphyrin dyes. Meanwhile, the cosensitizers are also effective in suppressing the dye aggregation for further improving the photovoltaic performance of porphyrin based DSSCs.[29–31] In this respect, we have reported various porphyrin dyes and their corresponding cosensitizers, such as **XW4** and **C1**,[14] **XW11** and **WS-5**,[13] **XW40** and **Z1**[11] using the I^-/I_3^- redox couple as the electrolyte.

Very recently, we reported efficient DSSCs based on **XW66** and **WS-5** using a cobalt electrolyte.[25] However, only a low photocurrent density (J_{sc}) of 8.97 mA cm^{-2} was obtained for **WS-5**, which may be ascribed to the relatively low molar absorption coefficients and the reduced charge collection

[a] *East China Sea Fisheries Research Institute, Chinese Academy of Fishery Sciences, Jungong 300, Shanghai 200090, P. R. China*
[b] *Key Laboratory for Advanced Materials and Institute of Fine Chemicals, School of Chemistry and Molecular Engineering, East China University of Science and Technology, Meilong 130, Shanghai 200237, P. R. China. E-mail: yshxie@ecust.edu.cn*

† Electronic supplementary information (ESI) available. See DOI: 10.1039/d1nj04797c

‡ These authors contributed equally to this work.

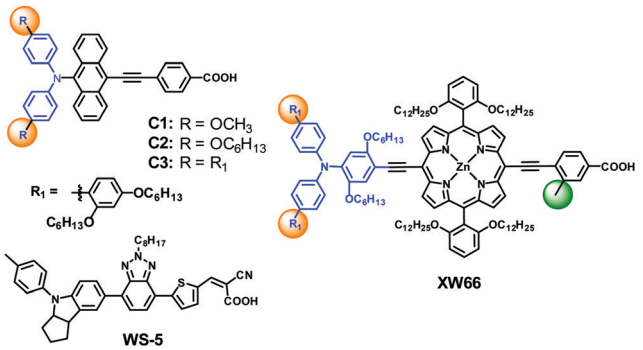

Fig. 1 Molecular structures of **C1–C3**, **WS-5** and **XW66**.[25]

efficiency resulting from the faster interfacial charge recombination in the cobalt-based redox electrolyte.[16] To address this problem, it may be feasible to develop organic dyes with higher molar absorption coefficients and more flexible substituents as the cosensitizers. In this respect, we have reported an anthracene-based **C1** utilizing a diphenylamine donor, which exhibits higher molar absorption coefficients within 350–600 nm relative to **WS-5**.[25] Thus, further modification of **C1** may be effective for designing efficient cosensitizers with higher J_{sc}. Based on this consideration, we herein report novel dyes **C2** and **C3** as cosensitizers for porphyrins by introducing bulky substituents in the diphenylamine unit of **C1** (Fig. 1). Compared with **C1**, the two hexyloxy chains introduced in the donor could effectively broaden the absorption, as well as hamper the adverse charge recombination process. Thus, an obviously higher J_{sc} of 13.03 mA cm^{-2} has been obtained for **C2** relative to that of 11.92 mA cm^{-2} obtained for **C1**. As a result, **C2** shows an improved efficiency of 7.59%. On this basis, **C3** has been synthesized by introducing two bulky dihexyloxyphenyl groups in the donor aiming to improve the photovoltage (V_{oc}), reducing the charge recombination between injected electrons and Co^{3+} ions or cations at the TiO_2/electrolyte interface. As expected, **C3** affords an improved V_{oc} of 857 mV relative to that of 843 mV obtained for **C1**. Meanwhile, the branched structure of **C3** is favorable for suppressing the interfacial back electron transfer and thus increases the J_{sc} to 13.23 mA cm^{-2}. As a result, the highest PCE value of 8.95% is achieved for **C3**, which is strikingly higher than those of 7.46% for **C1** and 5.02% for **WS-5**. Then, **C1–C3** were used as cosensitizers along with the porphyrin sensitizer **XW66**[25] to enhance the photocurrents by filling up the light absorption valleys of porphyrin dyes. As a result, the cells cosensitized with **C3** and **XW66** successfully afforded a remarkable efficiency of 10.22%. These results provide an effective strategy for designing efficient cosensitizers for porphyrin dyes.

Results and discussion

Syntheses of the organic dyes

The synthetic routes for organic dyes **C1–C3** are depicted in Scheme 1. **C1** was obtained according to our previous approach.[14] For **C2** and **C3**, the substituted diphenylamine moieties were synthesized according to the reported procedures,[25,32] which were then reacted with 9-bromoanthracene *via* Buchwald coupling reactions to afford the anthracene-based intermediates. The subsequent bromination and Sonogashira coupling reactions resulted in the ester derivatives of the dyes. Finally, **C2** and **C3** were achieved after hydrolysis of the esters under basic conditions.

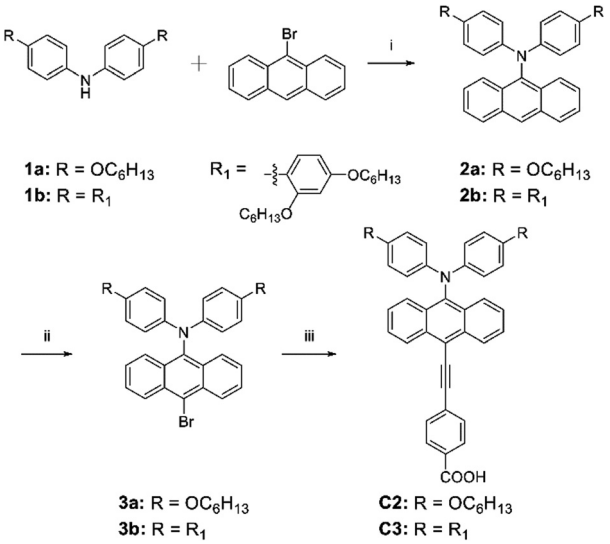

Scheme 1 Synthetic routes for **C2** and **C3**. Reaction conditions: (i) $Pd_2(dba)_3$, BINAP, *t*-BuONa, xylene. Yields: 68% for **2a**; 79% for **2b**; (ii) NBS, CH_2Cl_2. Yields: 30% for **3a**; 23% for **3b**; and (iii) (a) methyl 4-ethynylbenzoate, $Pd(PPh_3)_2Cl_2$, CuI, Et_3N, THF; (b) LiOH·H_2O, THF/H_2O. Yields: 72% for **C2**; 33% for **C3**.

Photophysical properties

The UV-vis absorption spectra of **C1–C3** in THF are shown in Fig. 2, and the corresponding data are summarized in Table 1. The absorption spectra of **C1–C3** show two absorption bands in the wavelength ranges of 350–450 nm and 450–600 nm assignable to the π–π* transition and intramolecular charge transfer (ICT) bands, respectively. The ICT band observed for **C2** at

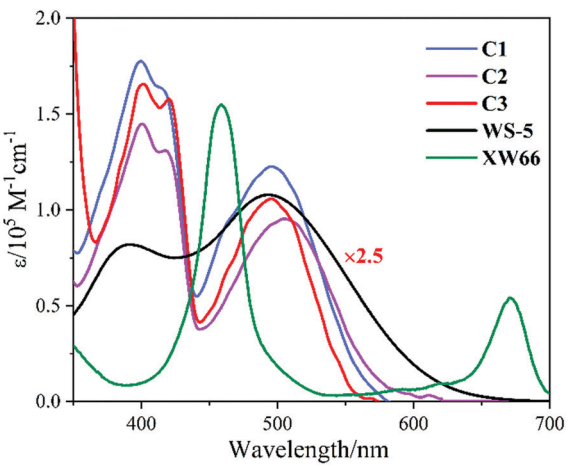

Fig. 2 Absorption spectra of **C1–C3**, **WS-5** and **XW66** in THF.

Table 1 Absorption and emission data of **C1–C3** in THF

Dyes	Absorption[a] λ_{max}/nm ($\varepsilon/10^3$ M^{-1} cm^{-1})	Emission[b] λ_{max}/nm
C1	399 (71.2), 417 (65.2), 495 (49.2)	649
C2	401 (57.6), 420 (52.4), 506(38.2)	653
C3	400 (66.4), 418 (62.8), 496 (42.4)	626

[a] Absorption maxima in THF solutions (2×10^{-6} M). [b] Excitation wavelengths/nm: 506 nm (**C2**), 496 nm (**C3**).

506 nm is red-shifted by *ca.* 11 nm relative to that of **C1** (495 nm), which may be ascribed to the presence of two electron-donating hexyloxy chains on the diphenylamine donor.[33,34] Compared with **C2**, the corresponding absorption peak of **C3** appears at 496 nm, which is only slightly red-shifted relative to that of **C1**, which may be ascribed to the lower electron-donating effect of the dihexyloxyphenyl groups in **C3** induced by the severe distortion between the directly linked phenyl moieties.[35,36] It is noteworthy that the molar absorption coefficients in 350–435 nm obtained for **C1–C3** are significantly higher than that of **WS-5**,[25] indicating that **C1–C3** may afford higher J_{sc} values than that of **WS-5**. When the dyes are adsorbed onto the TiO_2 film, the absorption peaks show blue shifts (Fig. S2, ESI†) as compared to those in the solutions, which may be ascribed to the H-aggregation of the dyes or the deprotonation of the carboxylic moiety accompanied by the adsorption onto the TiO_2 surface.[37,38] Despite the blue shifts, the broadened absorption peaks are beneficial for improving the light-harvesting ability.[36]

Electrochemical properties

Cyclic voltammetry was conducted to evaluate the feasibility of charge injection and dye regeneration for **C1–C3** (Fig. S3, ESI†), which play a crucial role in realizing the photovoltaic behavior of DSSCs.

As shown in Table S1 (ESI†), the estimated ground-state oxidation potentials (E_{OX}) were found to be 0.79, 0.79 and 0.94 V for **C1** to **C3** *versus* the normal hydrogen electrode (NHE), respectively, corresponding to the highest occupied molecular orbital (HOMO) energy levels (Fig. 3). It could be found that the HOMO levels of **C1–C3** are obviously more positive than the Co^{2+}/Co^{3+} redox couple (~0.56 V *vs.* NHE), indicating that the oxidized dyes can be efficiently regenerated by the electrolyte.[39] Moreover, **C3** exhibits a more positive HOMO level than those of other dyes, resulting in more efficient charge regeneration due to the larger energy gap.[36] The band gaps E_{0-0} of **C1–C3** were calculated to be 2.18 eV for **C1** and **C2**, and 2.24 eV for **C3**, respectively. The excited-state oxidation potentials (E^*_{OX}), calculated from $E_{OX} - E_{0-0}$, lie in the range of −1.30 to −1.39 V, considerably more negative than the conduction band edge (CB) of TiO_2 (−0.5 V *vs.* NHE), indicative of efficient electron injection into the TiO_2 conduction band from the excited sensitizers.[40] With enough driving forces for both charge injection and dye regeneration, **C1–C3** are expected to perform well in DSSCs based on the cobalt electrolyte.

Theoretical calculations

To obtain further insight into the electron distribution for **C1–C3**, density functional theory (DFT) and time-dependent density functional theory (TDDFT) calculations have been performed at the B3LYP/6-31G* level using the Gaussian 09 program package.[41–44] Thus, the molecular orbital profiles of **C1–C3** are shown in Fig. 4. The simulated E_{LUMO} and E_{HOMO} levels of the dyes (Table S2, ESI†) are consistent with the experimental values. According to the optimized structures, the HOMO levels of all the dyes are located on the electron donor units and the anthracene moiety, and the lowest unoccupied molecular orbitals (LUMOs) are mainly located on the anthracene moiety and the electron acceptor unit. The overlapping between the HOMO and LUMO is beneficial for electron injection from the dyes to the TiO_2 surface. In addition, the optimized structure of **C3** (Fig. S5, ESI†) displays a large dihedral angle of 55.1° between the terminal phenyl moieties and the phenylene moieties in the diphenylamine unit resulting in a much weaker ICT effect relative to **C2**, which is consistent with the relatively blue-shifted absorption of **C3** (*vide supra*).

Photovoltaic performance of the DSSCs

Based on the aforementioned results, DSSC devices were fabricated using **C1–C3** as the sensitizers and a cobalt electrolyte.

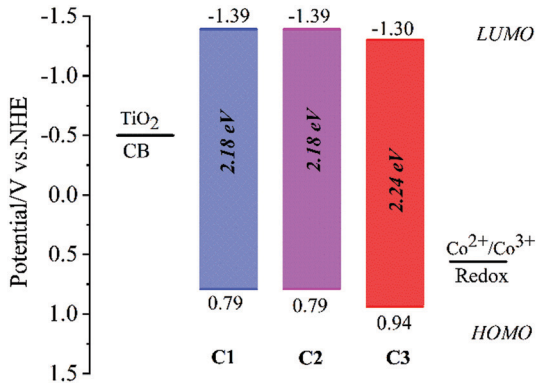

Fig. 3 Schematic energy level diagrams of **C1–C3**.

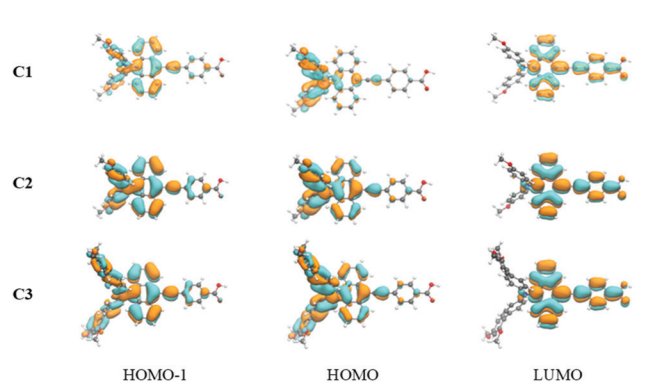

Fig. 4 Frontier molecular orbital profiles of **C1–C3** calculated using DFT.

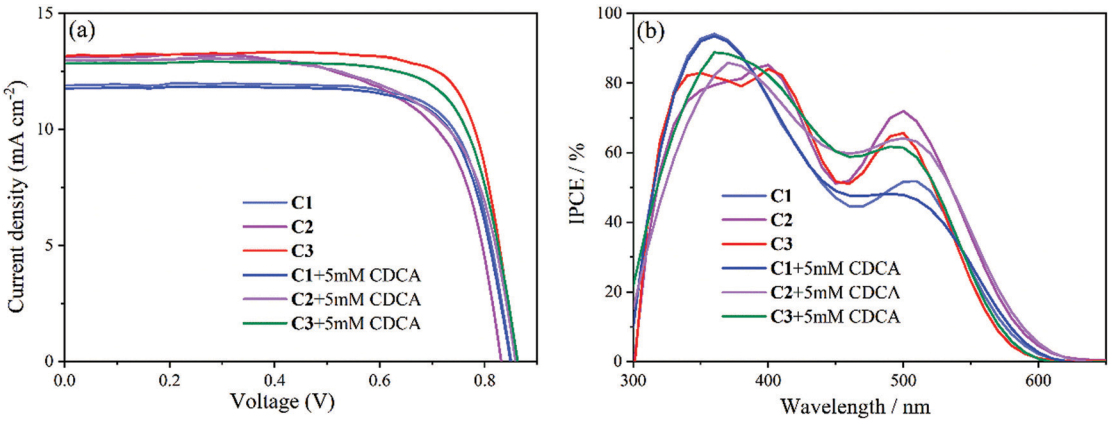

Fig. 5 (a) *J*–*V* curves and (b) IPCE spectra of solar cells sensitized with **C1–C3** in the absence/presence of 5 mM CDCA.

The photocurrent density–photovoltage (*J*–*V*) curves and monochromatic incident photon to current conversion efficiency (IPCE) spectra of the DSSCs are presented in Fig. 5, with the corresponding photovoltaic parameters listed in Table 2.

As shown in Fig. 5, the IPCE spectra of **C1–C3** are significantly broadened in the range of 350–635 nm, indicating that all the dyes can efficiently convert visible light into photocurrent. It is obvious that **C2** exhibits a red-shifted IPCE onset wavelength of *ca.* 635 nm relative to that of *ca.* 618 nm for **C1**, which may be ascribed to the strengthened ICT effect, resulting from the electron-donating effect of the two hexyloxy chains.[15] This observation is beneficial for enhancing the light-harvesting ability and thus generates a higher photocurrent of 13.03 mA cm^{-2}. Moreover, **C2** and **C3** exhibit IPCE plateaus up to 80% in the range of 350–430 nm and a strikingly higher plateau in 400–635 nm than that of **C1**. On the other hand, the hexyloxy and bulky groups introduced into **C2** and **C3** may effectively retard the charge recombination from the cobalt electrolyte and thus enhance the electron-collection yields, resulting in improved J_{sc} values of 13.03 mA cm^{-2} and 13.23 mA cm^{-2},[16] respectively, higher than those of 11.92 mA cm^{-2} for **C1** and 8.97 mA cm^{-2} for **WS-5**.[25] Hence, **C2** exhibits a conversion efficiency of 7.59%, which is higher than that of 7.46% for **C1**. In spite of the identical π-conjugation backbones, the V_{oc} value of 857 mV achieved for **C3** is dramatically higher than that of 843 mV obtained for **C1**, implying that the bulky substituents attached at the donor can efficiently suppress the recombination process for the electrons injected into the TiO_2 conduction band and the oxidized species in the electrolyte. Meanwhile, the bulky groups with large steric hindrance may aid in suppressing the harmful π···π stacking among the anthracene moieties. As a result, **C3** affords the highest efficiency of 8.95%, which is obviously higher than that of 5.02% for **WS-5**.

Chenodeoxycholic acid (CDCA) is usually co-adsorbed onto the surface of TiO_2 films as a nonchromophoric coadsorbent to suppress the dye aggregation and improve the photovoltaic behavior of DSSCs.[45] Thus, the photovoltaic properties of the DSSCs with co-adsorption of various concentrations of CDCA were investigated (Table S6, ESI†). As expected, the coadsorption of CDCA results in better V_{oc} than the individual dyes for **C1** and **C2**, along with the decreased J_{sc} values induced by the competitive adsorption of CDCA.[22] As a result, the efficiencies for the cells of **C1** and **C2** are enhanced to 7.52 and 7.84%, respectively, by using 5 mM CDCA. Unfortunately, decreased J_{sc} and PCE values were observed for **C3** when CDCA was applied, in comparison with those of the devices without using CDCA, as a result of reduced dye loading amounts on the TiO_2 surface.[33]

Table 2 Photovoltaic parameters of the DSSCs based on **C1–C3** under simulated AM1.5G full sun illumination (power 100 mW cm^{-2}) using the cobalt-based electrolyte

Dyes[a]	V_{oc}/V	J_{sc}/mA cm^{-2}	FF/%	PCE/%
C1	0.843 ± 0.005	11.92 ± 0.13	74.20 ± 0.31	7.46 ± 0.07
C2	0.831 ± 0.005	13.03 ± 0.38	70.14 ± 0.27	7.59 ± 0.24
C3	0.857 ± 0.002	13.23 ± 0.12	78.93 ± 1.49	8.95 ± 0.12
C1 + 5 mM CDCA	0.847 ± 0.008	11.79 ± 0.14	75.31 ± 0.25	7.52 ± 0.23
C2 + 5 mM CDCA	0.852 ± 0.002	12.89 ± 0.29	71.41 ± 0.31	7.84 ± 0.20
C3 + 5 mM CDCA	0.863 ± 0.004	12.73 ± 0.12	74.57 ± 0.21	8.19 ± 0.31
C1 + **XW66**	0.848 ± 0.004	15.03 ± 0.15	71.03 ± 0.15	9.06 ± 0.19
C2 + **XW66**	0.835 ± 0.006	16.35 ± 0.30	72.43 ± 0.10	9.89 ± 0.33
C3 + **XW66**	0.853 ± 0.009	16.95 ± 0.24	71.57 ± 0.19	10.22 ± 0.29
XW66	0.849 ± 0.002	14.87 ± 0.17	73.61 ± 0.20	9.23 ± 0.06
WS-5	0.867 ± 0.003	8.97± 0.22	65.52 ± 0.31	5.02 ± 0.13

[a] The parameters were obtained from the average value of five parallel devices. The active area is 0.12 cm^2.

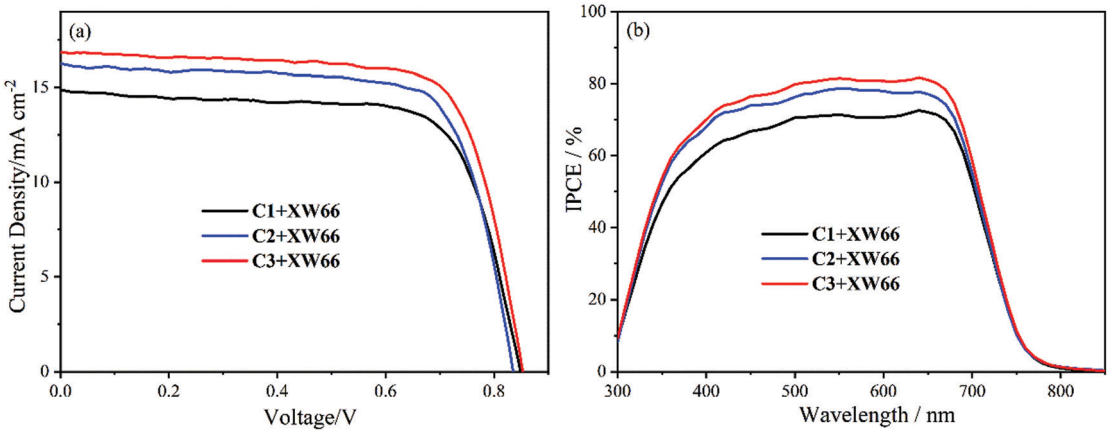

Fig. 6 (a) *J*–*V* curves and (b) IPCE spectra of the cells cosensitized with **C1–C3** and **XW66**.

Thus, **C1–C3** afforded the PCEs of 7.52–8.95% under the optimized conditions. For comparison, **C1–C3** were also used for fabricating solar cells based on the iodine electrolyte (Table S5, ESI†), which afforded lower efficiencies due to the much lower V_{oc} values.[31]

Considering the relatively high efficiencies obtained for **C1–C3**, they may be used as promising cosensitizers for porphyrin dyes, and thus they were further used as cosensitizers for the reported porphyrin dye **XW66** (Fig. 6 and Table 2).[25] As shown in Fig. 2, it is obvious that a series of valleys around 400 nm and 500–600 nm in the absorption spectra of **XW66** are well filled up by the contribution of **C1–C3**. Consistently, broad plateaus are observed in the IPCE spectra within a broad wavelength range of 400–690 nm, dramatically enhanced relative to the individual porphyrin dye **XW66**.[25] As a result, higher J_{sc} values of 15.03, 16.35 and 16.95 mA cm^{-2} are achieved for **XW66** + **C1–C3**, respectively. As a result of the strikingly enhanced photocurrents, **XW66** + **C1–C3** afforded improved PCEs of 9.06%, 9.89% and 10.22%, respectively. It is noteworthy that the highest PCE of 10.22% is much higher than that of 9.23% obtained for **XW66** individually.

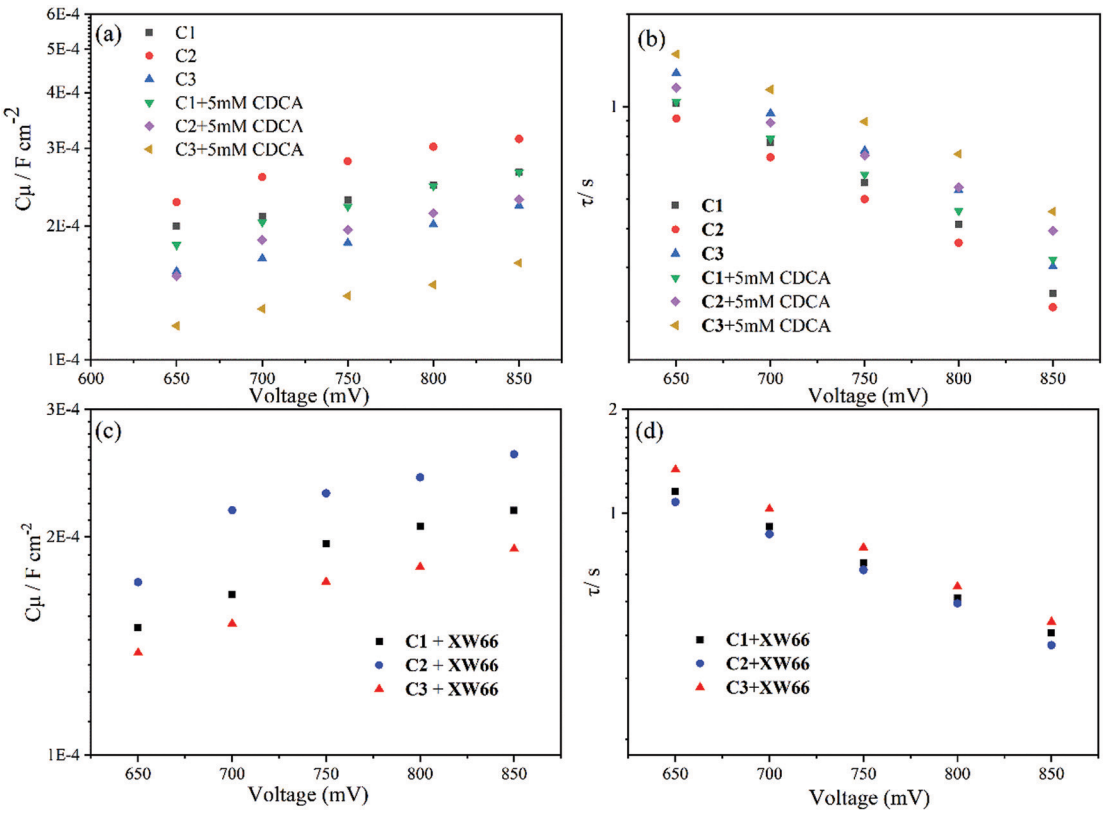

Fig. 7 Plots of (a and c) C_μ and (b and d) τ *vs.* potential bias for the DSSCs based on **C1–C3** and **XW66** + **C1–C3**.

Electrochemical impedance spectroscopy

To further understand the V_{oc} variation trend of the DSSCs, electrochemical impedance spectroscopy (EIS) was performed in the dark for a series of bias voltages. As is known, when a certain redox electrolyte is used for fabricating the devices, the V_{oc} values of DSSCs are related to the TiO_2 conduction band edges (E_{CB}) and the charge recombination processes, which can be revealed by the chemical capacitance (C_μ) and the electron lifetimes (τ), respectively (Fig. 7).[46,47] Thus, C_μ and τ values were obtained from electrochemical measurements. As shown in Fig. 7a, it is obvious that **C3** exhibits a strikingly lower C_μ value than those of **C1** and **C2** at a fixed forward bias, which indicates more negative shifts of the E_{CB} for **C3**, which is favorable for improving the V_{oc}. As a result, the C_μ values in the order of **C3** < **C1** < **C2** are in accordance with the sequence of the decreasing V_{oc} values. On the other hand, the τ values lie in the order of **C2** < **C1** < **C3** (Fig. 7b), indicative of the increasing electron lifetimes and decreasing charge recombination rates, which agree well with the observed increasing V_{oc} values of the DSSC devices. The longest τ values observed for **C3** may be ascribed to the superior anti-aggregation ability of the bulky groups and suppression of the charge recombination between the injected electrons and cations at the TiO_2/electrolyte interface.[48] These observations indicate that the V_{oc} variations of **C1–C3** are simultaneously governed by both the TiO_2 conduction band edges and the charge recombination processes. After coadsorption with CDCA, the devices based on **C1–C3** exhibit obviously decreased C_μ values, indicating an upward shift of the TiO_2 conduction band edge, favorable for improving the V_{oc}. Meanwhile, prolonged electron half-lifetimes are observed. It could be inferred that CDCA helps in relieving the aggregation and charge recombination problems for **C1–C3**. For the cosensitized **XW66** + **C1–C3** systems, the C_μ variation trend is similar to that observed for the individual dyes **C1–C3**, which is in accordance with that of the V_{oc} values (Fig. 7c). On the other hand, the cosensitized DSSCs exhibit quite similar τ values, indicative of little influence of the charge recombination processes (Fig. 7d). These results reveal that the V_{oc} values are mainly governed by the variation of the TiO_2 conduction band edges after cosensitization.

Conclusions

In summary, with the purpose of developing suitable cosensitizers for porphyrin dyes based on the cobalt electrolyte, novel anthracene dyes **C2** and **C3** have been designed and synthesized based on our previously reported cosensitizer **C1** by modifying the diphenylamine donor with hexyloxy chains and bulky dihexyloxyphenyl moieties, respectively. Thus, the electron-donating hexyloxy chains obviously broaden the absorption spectrum of **C2**, resulting in an improved J_{sc} of 13.03 mA cm^{-2} and a slightly higher PCE of 7.59% than those of **C1**. On the other hand, the two bulky dihexyloxyphenyl groups on the diphenylamine donor of **C3** exhibit superior anti-aggregation ability and retardation of the Co^{3+}/Co^{2+} ions from approaching the TiO_2 surface. As a result, the highest V_{oc} of 857 mV and PCE of 8.95% were obtained for **C3**. Upon coadsorption with CDCA, the efficiencies of **C1** and **C2** are improved to 7.52% and 7.84%, respectively. On this basis, **C1–C3** were used as cosensitizers for **XW66** to afford high efficiencies of 9.06–10.22%. In spite of the relatively high J_{sc} and PCE obtained for **XW66** + **C3**, this system still exhibits a slightly lower PCE than that of **XW66** + **WS-5** due to the lower V_{oc} of **C3** than that of **WS-5**, and thus **C3** could be further optimized and used as a cosensitizer for porphyrin dyes to achieve better photovoltaic performance in our future work. In one sentence, these results provide an effective approach for developing efficient cosensitizers for porphyrin dyes.

Author contributions

Writing – original draft preparation, Y. Y. T. and G. X. Y.; formal analysis, X. Y. L.; resources, Y. S. X.; data curation, Y. Y. T. and C. J. L.; writing – review and editing, D. M. H. and Y. S. X. All authors have read and agreed to the published version of the manuscript.

Conflicts of interest

There are no conflicts to declare.

Acknowledgements

This work was supported by Central Public-interest Scientific Institution Basal Research Fund, ECSFR, CAFS (2018T02), Shanghai Sailing Program (19YF1459900), NSFC (21772041, 21811530005, 21971063, U1707602), and the Fundamental Research Funds for the Central Universities (WK1616004, 222201717003).

Notes and references

1 B. O'Regan and M. Grätzel, *Nature*, 1991, **353**, 737–740.
2 H. Song, Q. Liu and Y. Xie, *Chem. Commun.*, 2018, **54**, 1811–1824.
3 I. Obraztsov, W. Kutner and F. D'Souza, *Sol. RRL*, 2017, **1**, 1600002.
4 L. L. Li and E. W. G. Diau, *Chem. Soc. Rev.*, 2013, **42**, 291–304.
5 N. Tomar, A. Agrawal, V. S. Dhaka and P. K. Surolia, *Sol. Energy*, 2020, **207**, 59–76.
6 M. K. Nazeeruddin, F. De Angelis, S. Fantacci, A. Selloni, G. Viscardi, P. Liska, S. Ito, B. Takeru and M. Grätzel, *J. Am. Chem. Soc.*, 2005, **127**, 16835–16847.
7 Q. Chai, W. Li, Y. Wu, K. Pei, J. Liu, Z. Geng, H. Tian and W. Zhu, *ACS Appl. Mater. Interfaces*, 2014, **6**, 14621–14630.
8 C. L. Wang, M. Zhang, Y. H. Hsiao, C. K. Tseng, C. L. Liu, M. Xu, P. Wang and C. Y. Lin, *Energy Environ. Sci.*, 2016, **9**, 200–206.

9 T. Hua, Z. S. Huang, K. Cai, L. Wang, H. Tang, H. Meier and D. Cao, *Electrochim. Acta*, 2019, **302**, 225–233.
10 K. Zeng, Y. Chen, W. Zhu, H. Tian and Y. Xie, *J. Am. Chem. Soc.*, 2020, **142**, 5154–5161.
11 K. Zeng, Y. Lu, W. Tang, S. Zhao, Q. Liu, W. Zhu, H. Tian and Y. Xie, *Chem. Sci.*, 2019, **10**, 2186–2192.
12 K. Zeng, W. Tang, C. Li, Y. Chen, S. Zhao, Q. Liu and Y. Xie, *J. Mater. Chem. A*, 2019, **7**, 20854–20860.
13 Y. Xie, Y. Tang, W. Wu, Y. Wang, J. Liu, X. Li, H. Tian and W. H. Zhu, *J. Am. Chem. Soc.*, 2015, **137**, 14055–14058.
14 Y. Wang, B. Chen, W. Wu, X. Li, W. Zhu, H. Tian and Y. Xie, *Angew. Chem., Int. Ed.*, 2014, **53**, 10779–10783.
15 Y. Tang, Y. Wang, X. Li, H. Ågren, W. H. Zhu and Y. Xie, *ACS Appl. Mater. Interfaces*, 2015, **7**, 27976–27985.
16 A. Yella, H. W. Lee, H. N. Tsao, C. Yi, A. K. Chandiran, M. K. Nazeeruddin, E. W. G. Diau, C. Y. Yeh, S. M. Zakeeruddin and M. Grätzel, *Science*, 2011, **334**, 629–634.
17 J. Liu, R. Li, X. Si, D. Zhou, Y. Shi, Y. Wang, X. Jing and P. Wang, *Energy Environ. Sci.*, 2010, **3**, 1924–1928.
18 T. Wei, X. Sun, X. Li, H. Ågren and Y. Xie, *ACS Appl. Mater. Interfaces*, 2015, **7**, 21956–21965.
19 S. Mathew, A. Yella, P. Gao, R. Humphry-Baker, F. E. CurchodBasile, N. Ashari-Astani, I. Tavernelli, U. Rothlisberger, K. NazeeruddinMd and M. Grätzel, *Nat. Chem.*, 2014, **6**, 242–247.
20 A. Yella, C. L. Mai, S. M. Zakeeruddin, S. N. Chang, C. H. Hsieh, C. Y. Yeh and M. Grätzel, *Angew. Chem., Int. Ed.*, 2014, **53**, 2973–2977.
21 Y. Lu, Q. Liu, J. Luo, B. Wang, T. Feng, X. Zhou, X. Liu and Y. Xie, *ChemSusChem*, 2019, **12**, 2802–2809.
22 Y. Lu, H. Song, X. Li, H. Ågren, Q. Liu, J. Zhang, X. Zhang and Y. Xie, *ACS Appl. Mater. Interfaces*, 2019, **11**, 5046–5054.
23 H. Song, J. Zhang, J. Jin, H. Wang and Y. Xie, *J. Mater. Chem. C*, 2018, **6**, 3927–3936.
24 H. Song, X. Li, H. Ågren and Y. Xie, *Dyes Pigm.*, 2017, **137**, 421–429.
25 Y. Tang, Y. Wang, Q. Yan, K. Zeng, W. Tang, S. Zhao, C. Kong and Y. Xie, *Dyes Pigm.*, 2021, **187**, 109075.
26 Y. Tang, X. Liu, Y. Wang, Q. Liu, X. Li, C. Li, X. Shen and Y. Xie, *Chin. Chem. Lett.*, 2020, **31**, 1927–1930.
27 Y. Tang, Y. Wang, H. Song, Q. Liu, X. Li, Y. Cai and Y. Xie, *Dyes Pigm.*, 2019, **171**, 107776.
28 J. F. Lu, X. B. Xu, Z. H. Li, K. Cao, J. Cui, Y. Zhang, Y. Shen, Y. Li, J. Zhu, S. Y. Dai, W. Chen, Y. B. Cheng and M. K. Wang, *Chem. – Asian J.*, 2013, **8**, 956–962.
29 J. Luo, M. Xu, R. Li, K. Huang, C. Jiang, Q. Qi, W. Zeng, J. Zhang, C. Chi, P. Wang and J. Wu, *J. Am. Chem. Soc.*, 2014, **136**, 265–272.
30 X. Sun, Y. Wang, X. Li, H. Ågren, W. Zhu, H. Tian and Y. Xie, *Chem. Commun.*, 2014, **50**, 15609–15612.
31 Y. Lu, Y. Cheng, C. Li, J. Luo, W. Tang, S. Zhao, Q. Liu and Y. Xie, *Sci. China: Chem.*, 2019, **62**, 994–1000.
32 K. D. Seo, B. S. You, I. T. Choi, M. J. Ju, M. You, H. S. Kang and H. K. Kim, *Dyes Pigm.*, 2013, **99**, 599–606.
33 Y. Hua, B. Jin, H. Wang, X. Zhu, W. Wu, M. Cheung, Z. Lin, W. Wong and W. Wong, *J. Power Sources*, 2013, **237**, 195–203.
34 G. Marzari, J. Durantini, D. Minudri, M. Gervaldo, L. Otero, F. Fungo, G. Pozzi, M. Cavazzini, S. Orlandi and S. Quici, *J. Phys. Chem. C*, 2012, **116**, 21190–21200.
35 D. Hagberg, X. Jiang, E. Gabrielsson, M. Linder, T. Marinado, T. Brinck, A. Hagfeldt and L. Sun, *J. Mater. Chem.*, 2009, **19**, 7232–7238.
36 J. Zhao, X. Yang, M. Cheng, S. Li, X. Wang and L. Sun, *J. Mater. Chem. A*, 2013, **1**, 2441–2446.
37 F. R. Dai, Y. C. Chen, L. F. Lai, W. J. Wu, C. H. Cui, G. P. Tan, X. Z. Wang, J. T. Lin, H. Tian and W. Y. Wong, *Chem. – Asian J.*, 2012, **7**, 1426–1434.
38 A. Hagfeldt and M. Grätzel, *Acc. Chem. Res.*, 2000, **33**, 269–277.
39 Y. Cheng, G. Yang, H. Jiang, S. Zhao, Q. Liu and Y. Xie, *ACS Appl. Mater. Interfaces*, 2018, **10**, 38880–38891.
40 G. Yang, Y. Tang, X. Li, H. Ågren and Y. Xie, *ACS Appl. Mater. Interfaces*, 2017, **9**, 36875–36885.
41 W. J. Hehre, R. Ditchfield and J. A. Pople, *J. Chem. Phys.*, 1972, **56**, 2257–2261.
42 A. D. Becke, *J. Chem. Phys.*, 1993, **98**, 5648–5652.
43 C. Lee, W. Yang and R. G. Parr, *Phys. Rev. B: Condens. Matter Mater. Phys.*, 1988, **37**, 785–789.
44 M. J. Frisch, G. W. Trucks, H. B. Schlegel, G. E. Scuseria, M. A. Robb, J. R. Cheeseman, G. Scalmani, V. Barone, B. Mennucci, G. A. Petersson, H. Nakatsuji, M. Caricato, X. Li, H. P. Hratchian, A. F. Izmaylov, J. Bloino, G. Zheng, J. L. Sonnenberg, M. Hada, M. Ehara, K. Toyota, R. Fukuda, J. Hasegawa, M. Ishida, T. Nakajima, Y. Honda, O. Kitao, H. Nakai, T. Vreven, J. A. Montgomery Jr, J. E. Peralta, F. Ogliaro, M. J. Bearpark, J. Heyd, E. N. Brothers, K. N. Kudin, V. N. Staroverov, R. Kobayashi, J. Normand, K. Raghavachari, A. P. Rendell, J. C. Burant, S. S. Iyengar, J. Tomasi, M. Cossi, N. Rega, N. J. Millam, M. Klene, J. E. Knox, J. B. Cross, V. Bakken, C. Adamo, J. Jaramillo, R. Gomperts, R. E. Stratmann, O. Yazyev, A. J. Austin, R. Cammi, C. Pomelli, J. W. Ochterski, R. L. Martin, K. Morokuma, V. G. Zakrzewski, G. A. Voth, P. Salvador, J. J. Dannenberg, S. Dapprich, A. D. Daniels, Ö. Farkas, J. B. Foresman, J. V. Ortiz, J. Cioslowski and D. J. Fox, *Gaussian 09, Revision A. 2*, Gaussian, Inc., Wallingford CT, 2009.
45 P. Wang, S. Zakeeruddin, S. Comte, R. Charvet, R. Humphrybaker and M. Grätzel, *J. Phys. Chem. B*, 2003, **107**, 14336–14341.
46 S. Kang, M. Jeong, Y. Eom, I. Choi, S. Kwon, Y. Yoo, J. Kim, J. Kwon, J. Park and H. Kim, *Adv. Energy Mater.*, 2017, **7**, 1602117.
47 Y. Shi, M. Liang, L. Wang, H. Han, L. You, Z. Sun and S. Xue, *ACS Appl. Mater. Interfaces*, 2013, **5**, 144–153.
48 L. Han, A. Islam, H. Chen, C. Malapaka, B. Chiranjeevi, S. Zhang, X. Yang and M. Yanagida, *Energy Environ. Sci.*, 2012, **5**, 6057–6060.